ARCHIVES OF ELECTRICAL ENGINEERING VOL. 69(3), pp. 521–543 (2020)

DOI 10.24425/aee.2020.133916

Simulation of the proposed combined Fuzzy Logic Control for Maximum Power Point Tracking and Battery Charge Regulation used in CubeSat

ABDERRAHMANE SEDDJAR[1], KAMEL DJAMEL EDDINE KERROUCHE[1], LINA WANG[2]

[1]*Algerian Space Agency, Satellites Development Center*
PO Box 4065, Ibn Rochd USTO, Bir El Djir, Oran, Algeria

[2]*School of Automation on Science and Electrical Engineering*
Beihang University, Beijing 100191, China
e-mail: aseddjar@cds.asal.dz

(Received: 24.11.2019, revised: 03.03.2020)

Abstract: One of the most critical systems of any satellite is the Electrical Power System (EPS) and without any available energy, the satellite would simply stop to function. Therefore, the presented research within this paper investigates the areas relating to the satellite EPS with the main focus towards the CubeSat platform. In this paper, an appropriate EPS architecture with the suitable control policy for CubeSat missions is proposed. The suggested control strategy combines two methods, the Maximum Power Point Tracking (MPPT) and the Battery Charge Regulation (BCR), in one power converter circuit, in order to extract the maximum power of the Photovoltaic (PV) system and regulate the battery voltage from overcharging. This proposed combined control technique is using a Fuzzy Logic Control (FLC) strategy serving two main purposes, the MPPT and BCR. Without an additional battery charger circuit and without switching technique between the two controllers, there are no switching losses and the efficiency of the charging characteristic can be increased by selecting this proposed combined FLC. By testing a space-based PV model with the proposed EPS architecture, some simulation results are compared to demonstrate the superiority of the proposed control strategy over the conventional strategies such as Perturb and Observe (P&O) and FLC with a Proportional Integral Derivative (PID) controller.

Key words: combined Fuzzy Logic Control, Electrical Power System, photovoltaic system, Maximum Power Point Tracking, Battery Charge Regulation, Perturb and Observe, CubeSat

1. Introduction

In the last decade, numerous versions of CubeSat platforms based on the CubeSat standard, such as 1Unit, 2Units and 3Units, have been built and put into orbit [1–4]. They have become an excellent alternative to tests new technologies with a reduced cost of manufacturing and launch. The structure of the studied CubeSat based 1.5 U standard is shown in Fig. 1.

Fig. 1. CubeSat based on 1.5 U platform [5]

During any CubeSat mission, the Electrical Power System (EPS) is the most important part of handling power conversion and battery charging, as well as ensuring controlled power to the rest of the CubeSat systems. The EPS of CubeSats has several circuit approaches that can mainly be divided into two main types; the Direct Energy Transfer (DET) circuit and the Peak Power Transfer (PPT) circuit [6]. All other topologies are dissimilarities, derivations or mixtures of these two main types. Meanwhile, both of these configurations have a common circuit in the arrangement of Photovoltaic (PV) solar panels (primary source) and power distribution units. The distinction between DET and PPT consists of the power electronics interfacing the PV source and storage system (secondary source). Nevertheless, the majority of CubeSat missions using the DET topology have an efficiency loss [7]. In Low Earth Orbit (LEO) real conditions, while the CubeSat's angle towards the sun continuously changes and the amount of solar flux incoming to solar cells varies significantly, the operation of the solar array at the maximum power point seems to be suitable solution [8]. Therefore, the PPT has more advantages for LEO missions less than 5 years life time that require more power at Beginning of Life (BOL) than at End of Life (EOL). The PPT is a non-dissipative circuit for the reason that it can extract a precise power, which is required by the CubeSat, up to the solar array's maximum power [7]. This PPT approach increases efficiency and simultaneously eliminates the potential of thermal dissipation problems encountered in the DET method from BOL to EOL.

During sunlight periods, Maximum Power Point Tracking (MPPT) control algorithms are used for PPT systems in space applications, which are quite similar to those used in ground applications. In the literature, several works focused on the development of MPPT's algorithms are studied such as Perturb and Observe (P&O) in [9–12], Incremental Conductance (INC) in [13–15], a single short pulse of loading [16], and the so-called intelligent control based on Fuzzy Logic (FL) in [17–19]. However, nowadays, the development of the adaptive and artificial intelligence techniques to

improve the efficiency of the PV system remains a challenging research field. Therefore, numerous algorithms based on intelligent techniques such as FL in [20–23] and the adaptive neural-fuzzy in [24–26] have been modified and developed. FL control techniques are appropriate for non-linear control as demonstrated in [27–29]. Unlike traditional controllers such as P&O and INC, FL Controllers (FLCs) are able to use experimental methods or professional knowledge to adjust the output control system even without understanding the mathematical model of the systems being controlled. In [30], a fuzzy controller for a maximum power point tracker and the hierarchical fuzzy sub-systems controller are proposed for a CubeSat. In [31], simulation and implementation of FLC based Maximum Power Point Tracking (MPPT) for different configurations of a partially shaded PV system are presented. A control strategy based on the traditional PI controller and intelligent fuzzy logic controller for power management of the DC micro grid consisting of PV modules and fuel cells is presented in [32]. In [31], a comparative analysis of different MPPT method including the fuzzy logic and the genetic algorithm techniques is presented.

During eclipse periods and peak-power demands, CubeSats are using batteries as a secondary power source. Available battery technologies used in space applications are those including Nickel-Metal Hydride (NiMH), Lithium-ion (Li-ion) and Li-ion Polymer (LiPo) [34]. Nevertheless, the only battery technology practicable for the CubeSat usage is that of Li-ion or LiPo, due to their high energy densities [35]. Since these secondary power systems require a management system for energy storage, but when the sunlight is brighter, PVs collect more power and excessive voltage can damage the batteries. Hence, in the EPS, the Battery Charger Regulation (BCR) block, which is responsible for implementing a Constant Voltage (CV) charging strategy, should be used to prevent the battery failure in order to prevent the battery from overcharging when it is already fully charged [36]. In [37], the design of a Buck-Boost converter with a PI controller is used in order to combine both hybrid power sources PV/Wind with a battery storage system. In [38], a PID controller is used for BCR with a conventional MPPT algorithm for the optimization of the power extraction. In [39], a Sliding Mode Control (SMC) strategy was used for the MPPT and the control of the battery voltage.

In the above literature, most of the proposed control strategies are based on two separated controllers (MPPT and BCR) with independent electrical circuits. However, the reliability of the EPS is reduced due to the complexity of the circuit with an additional battery charger and showing an ineffective coordination between these two controllers. Therefore, the proposed combined Fuzzy Logic Control strategy can be capable to place the operating point of the PV systems precisely on the MPPs and control the battery voltage at the rated value without state transition or switching mechanism between the MPPT and BCR controllers. Likewise, this proposed control strategy is dedicated directly to control one power converter circuit including both the MPPT and BCR techniques, which eliminates the need for extra battery charger.

The remaining part of this paper is organized as follows: Section 2 is dedicated to the proposed electrical architecture of the EPS for a CubeSat. Then, the operating principle and modelling of each EPS components (solar panel, boost converter and battery) are presented in the same section. The common issues of the conventional control strategies are discussed in Section 3. In Section 4, the proposed Fuzzy Logic Control strategy is presented. In Section 5, some simulation results obtained under different irradiances and temperatures conditions are presented to show the effectiveness of the proposed combined FLC approach. The conclusion and findings of the proposed work are discussed in Section 6.

2. Electrical Power System of the 1.5U Cubesat

In the 1.5U Cubesat EPS architecture, as shown in Fig. 2, the solar cells are placed on five sides. Instead of using one boost converter per side of the CubeSat, a good trade-off can be to use one boost converter for two solar panels on opposite sides. These solar panels are mounted on opposing faces of the CubeSat connected to the same power converter (–X array and +X array are connected to MPPT1, –Y and +Y to MPPT2 and +Z to MPPT3). The power converters are connected in parallel and each converter has an MPPT algorithm. In this configuration only one panel per pair can be directly illuminated by sun at any given time, with the second panel providing a limited amount of energy due to albedo illumination from the earth. This is very beneficial because it allows different MPPs to be tracked due to differences in irradiance and temperature in separate solar panels.

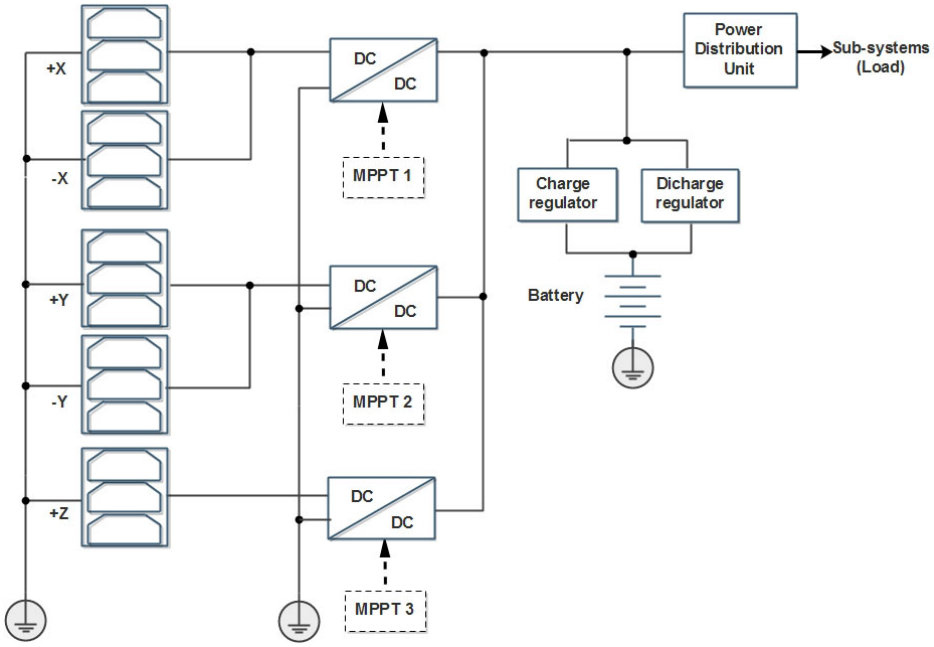

Fig. 2. EPS architecture of 1.5U CubeSat

2.1. Solar panel modelling

In this paper, a model of a solar panel has been developed using MATLAB/Simulink, the simplified model of the solar cell is shown in Fig. 3 as follows [40].

In the model D is the diode representing the PN junction polarization phenomena, R_s and R_{sh} are the series and shunt resistors representing losses. Based on the application of the Kirchhoff law in Fig. 3, the following equation is obtained:

$$I_{ph} = I_D + I_R + I, \tag{1}$$

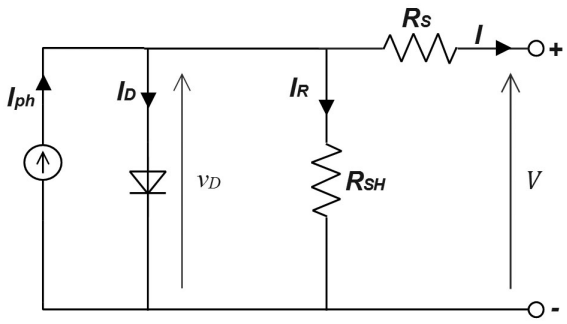

Fig. 3. Solar cell model

where:

$$I_D = I_0\left(e^{q\left(\frac{V+IR_s}{nKT}\right)} - 1\right), \qquad I_R = \frac{V + IR_s}{R_{SH}}. \tag{2}$$

The current generated by the solar cell has the following expression:

$$I = I_{ph} - I_0\left(e^{q\left(\frac{V+IR_s}{nKT}\right)} - 1\right) - \frac{V + IR_s}{R_{SH}}, \tag{3}$$

where: I_{ph} and I_0 are the current source and the saturation current of the diode, respectively. K is the Boltzmann constant (1.38×10^{-23} J/K); n is the ideality factor (from 1 to 2); T is the temperature (in Kelvin); q is the electron charge (1.6×10^{-19} C).

The current source has the following Equation (4):

$$I_{ph} = (I_{SC} + K_i\,(T - 298.15))\,\frac{G}{G_n}, \tag{4}$$

where: G and G_n are the irradiance and the refrerence irradiance, respectively. K_i is the temperature coefficient of short-circuit current. I_{SC} is the short-circuit current.

After simplification ($R_{SH} = \infty$) in (3), the following equation is obtained:

$$I = I_{SC} - I_0\left(e^{q\left(\frac{V+IR_s}{nKT}\right)} - 1\right). \tag{5}$$

Supposing $I = 0$, ($V = V_{oc}$), the following equation is obtained:

$$I_0 = I_{SC}e^{-\left(\frac{V_{oc}}{V_t}\right)}, \tag{6}$$

where: V_{oc} is the open-circuit output voltage. The voltage $V_t = \dfrac{nKT}{q}$.

After substitution of (6) in (5), the following equation is found:

$$I = I_{SC}\left(1 - e^{\left(\frac{V-V_{oc}-IR_s}{V_t}\right)}\right). \tag{7}$$

The parameters of the used solar cell model are listed in Appendix A.

In this study, for 1.5U CubeSat, three solar cells are connected in parallel in each solar panel. The generated power and the electrical characteristics of the solar panel depend on environmental conditions such as irradiances and temperatures. The electrical characteristics of the various photovoltaic panels existing on the space industry market are not identical.

2.2. Power converter

The configuration of the boost converter connected with the solar panel is shown in Fig. 4.

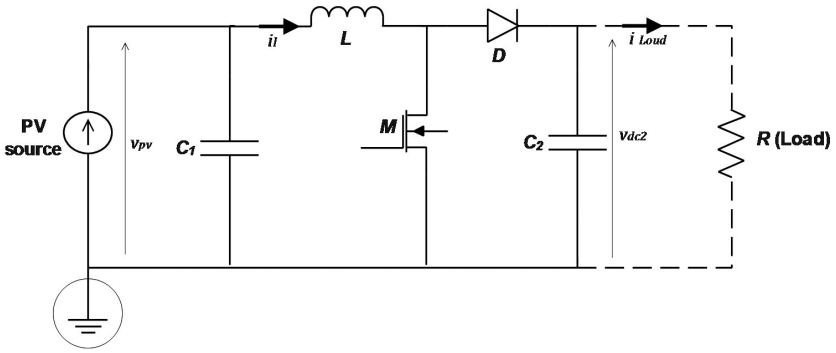

Fig. 4. Electrical scheme of the boost converter

The dynamic model of the boost DC–DC converter in state space form is found by the application of the equation of basic electronic laws, which is written in (8). [41]:

$$\frac{\mathrm{d}}{\mathrm{d}t}\begin{bmatrix} i_l \\ v_{dc2} \end{bmatrix} = \begin{bmatrix} 0 & -\dfrac{1}{L}(1-U) \\ \dfrac{1}{C_2}(1-U) & -\dfrac{1}{C_2 R} \end{bmatrix} \begin{bmatrix} i_l \\ v_{dc2} \end{bmatrix} + \begin{bmatrix} \dfrac{v_{pv}}{L} \\ 0 \end{bmatrix}, \tag{8}$$

where: v_{pv} is the voltage of the PV panel, v_{dc2} and $i_{load} = \dfrac{v_{dc2}}{R}$ are the output voltage and load current, respectively. $U \in \{0,\ 1\}$ is the switch state M. The parameters of the boost converter are presented in Appendix B.

3. EPS control strategy issue

As already mentioned in the introduction, many research works have implemented two independent controllers MPPT and BCR. Generally, this type of topology requires a supervisor to switch between these two controllers. The operating principle is shown in the following flowchart (Fig. 5):

Obviously, in the PV system, there is only one point on its electrical characteristic curve (P–V or I–V), called the Maximum Power Point (MPP), at which a maximum output power is produced. However, since the MPP varies with different levels of irradiance and temperature, it is difficult to maintain MPP operation at all these environmental conditions without changes in the system parameters. The MPPT algorithm aims to follow the MPP of a non-linear PV system, where, the maximum possible current depends on the solar irradiance received by the PV cell. Therefore, to increase the power, it is only possible to vary the voltage. The controlled variation of the voltage can be made by means of a DC–DC converter, while, by specific and well-defined algorithms, this automatic variation is ensured for its duty cycle.

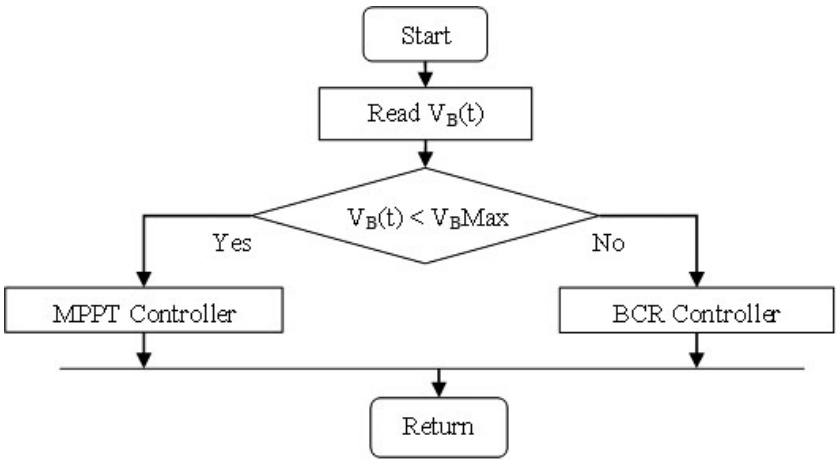

Fig. 5. Control strategy flowchart

The P&O method is the MPPT technique most widely used in PV systems because of its simplicity and easy implementation. The operating principle of this method is to generate a periodic disturbance of the operating voltage and observe its effect on the output power.

Generally, the commonly used MPPT techniques such as the P&O and INC methods use a fixed step for incrementing or disrupting the voltage. While, the choice of step value is a serious issue for these techniques for the following reasons:

– If the step value is large and conditions (temperature and irradiance) change rapidly, the MPPT algorithm will respond quickly and converge to the optimal operating point, but this causes ripples and considerable losses once these conditions are stable.
– If the step value is small, the losses and ripples under stable conditions will be reduced, but the system will not be able to follow the MPP under a sudden change in these conditions.

Therefore, to overcome these issues, the solution is to automatically and intelligently adjust the duty cycle step value by using one of the most efficient methods, which is the fuzzy logic theory. Compared to the traditional controllers such as P&O and INC, the FLC is capable to adjust the duty cycle of the power converter even without needing to understand the complex mathematical model of the system. However, it requires a professional knowledge to determine fuzzy inference rules.

The secondary control state of the EPS is BCR, which consists in regulating the battery voltage at a specific reference voltage with a PID controller. In this battery charge control loop, the pole placement method is used to calculate the PID controller parameters. These calculated controller parameters include the values of the designed boost converter parameters, such as inductance, capacitance and resistance. However, the stability of the closed-loop system is sensitive to variations in these parameters, which is a significant problem for controller robustness. Moreover, due to environmental effects in space and other disturbances (EMC and heating), system parameters are constantly changing. Therefore, the controller design must be independent of the system parameters to reduce its sensitivity, increase its robustness and ensure the stability of the system, which can be achieved by the use of the FLC theory.

A switch is included in the conventional control system to alternate between the two different controllers. Regardless the rapid function of this switch, the impact of switching from one controller to another will be visible, as well as the additional oscillations at the output system. In the case when the environmental conditions lead to a point where the voltage is close to the state of the switching condition, the switch will be a disruptive element and will import more significant oscillations in the system response. The ideal solution to avoid this unwanted impact related to the use of the switch is to combine the two controllers (MPPT and BCR) as suggested in this paper.

4. Proposed combined Fuzzy Logic Control

A combined Fuzzy Logic Control (FLC) is suggested based on two MPPT and BCR techniques to perform both tasks simultaneously. Fig. 6, shows the equivalent circuit of the EPS by using the proposed control strategy that allows the reduction of the typical EPS architecture (Fig. 2).

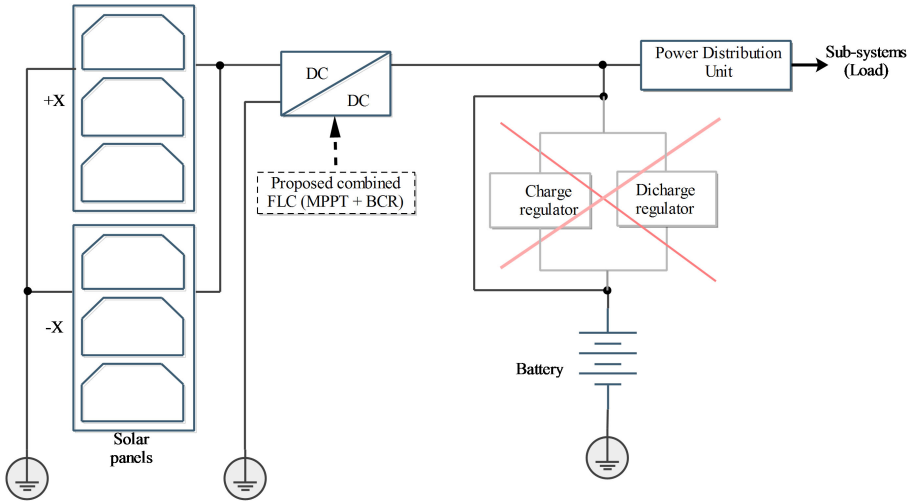

Fig. 6. Proposed equivalent EPS architecture

This proposed equivalent EPS architecture based on C-FLC not only allows for significant reduction of the ripples around the desired value (without switching between the two controllers) but also allows one to completely get rid of an additional electronic circuit. In CubSats, this optimization is crucial and brings several advantages such as power efficiency, less weight and more space [42]. Furthermore, the proposed C-FLC can be generalized for any CubeSat 1U to 6U. Whereas, a certain adaptation of the sizing parameters of the power converters is necessary depending on the size of the solar panels and the electrical characteristics of the CubeSat subsystems.

One of the advantages of the proposed C-FLC is the consideration of the duty cycle feedback as an input variable, which makes it possible to know precisely their position with respect to

the MPP. Then, the ripples around the MPP can be considerably reduced with improved MPP efficiency, flexibility and convergence speed.

The design of the FL system requires going through the steps of selecting fuzzy parameters, such as membership functions, the inferences method and the fuzzification strategy [43]; these steps which constituted the fuzzy logic controller are illustrated in Fig. 7.

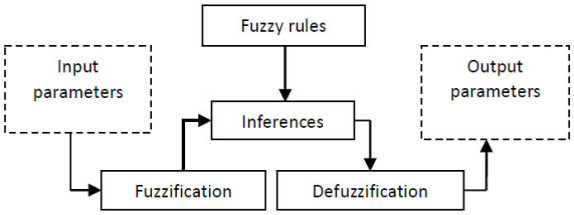

Fig. 7. Structure of fuzzy logic controller

The most common FL MPPT algorithms generate fuzzy input variables from PV system voltage and current signals. The fuzzy input variables would therefore be used to calculate the duty cycle control in order to adjust the operating point of the photovoltaic system to maximize the output power.

The proposed C-FLC algorithm has four input variables: ΔP is the variations of the power of the photovoltaic system, ΔV_B is the variation of the output voltage of the boost converter, V_B is the difference between the maximum battery voltage charging (V_BMAX) and the feedback of the instantaneous voltage ($V_B(k)$), D_{in} is the feedback of the duty cycle at instant $(K-1)$. While, the output is based on one variable D_{out} obtained by the addition (duty cycle $(K-1)$ + Delta duty cycle). Fig. 8 shows the flowchart of the fuzzy controller calculation process.

The choice of the fuzzification approach consists in defining the forms of membership functions and their arrangement in the universe of discourse. There are several forms of membership functions, such as the triangular shape, the trapezoidal shape and so on. Comparative studies of these different forms of membership functions have shown almost identical results [44]. However, triangular shapes are proportionally easy to program, which explains why they are the most used. In this proposed control strategy, for the membership functions, two forms at once are adopted, which are the triangular and trapezoidal forms.

The definition of membership functions for this combined FLC requires special knowledge of the system and consists in applying several tests. If the duty cycle membership functions are smaller than necessary, large overshoots and ripples on the battery voltage can be obtained. Otherwise, if the membership functions of the duty cycle are large, the desired battery voltage will be quickly maintained without ripples or overshoots, but with a slow response time. These effects can reduce battery lifetime, which directly affects the mission of the satellite. Therefore, suitable sizes of membership functions and right fuzzy rules need to be well defined.

In order to achieve an appropriate FL control to the proposed system, the following flowchart (Fig. 9) should be followed:

The membership functions for the input D_{in}, the inputs ΔP, V_B, $\Delta V_B(K)$ and the output D_{out} are shown in Fig. 10, Fig. 11 and Fig. 12, respectively. The input D_{in} is expressed by the following variables: VS (Very Small), SM (Small), M (Medium), FA (Fast), and VF (Very Fast).

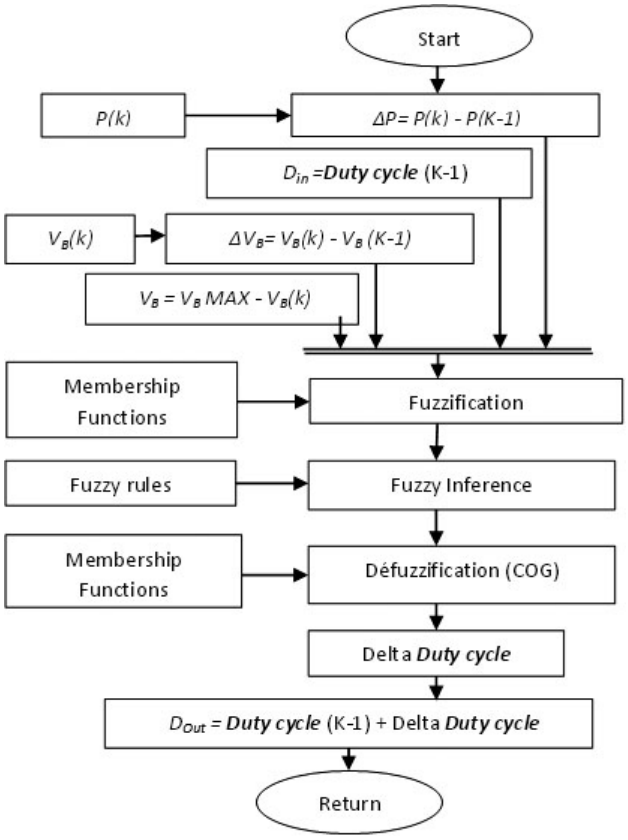

Fig. 8. Flowchart of proposed combined FLC algorithm

The inputs ΔP, V_B, $\Delta V_B(K)$ are expressed by the following variables: VL (Very Low), L (Low), M (Medium), H (High), and VH (Very High). The output variable D_{out} of the proposed method is expressed by five fuzzy membership functions: NM (Negative Minimum), N (Negative), CO (Correct), P (Positive), and PM (Positive Maximum).

The fuzzy rules have been defined based on the description of the system to be controlled, according to the linguistic variables and the membership functions for the inputs and output variables. A total of 50 rules (Appendix E) were used for the proposed combined FLC.

The Mamdani inference method [45] is adopted in this paper. The AND operator is performed by the calculation of the minimum, while the OR operator is performed by calculating the maximum. For the defuzzification method, the Centre of Gravity Method (COG) [45] is used, which is expressed as follows:

$$x_S = \frac{\int_x u_\beta(x) x \, \mathrm{d}x}{\int_x u_\beta(x) \, \mathrm{d}x}, \tag{9}$$

where: $u_\beta(x)$ is the membership function and x_S is the exact value of the FL output.

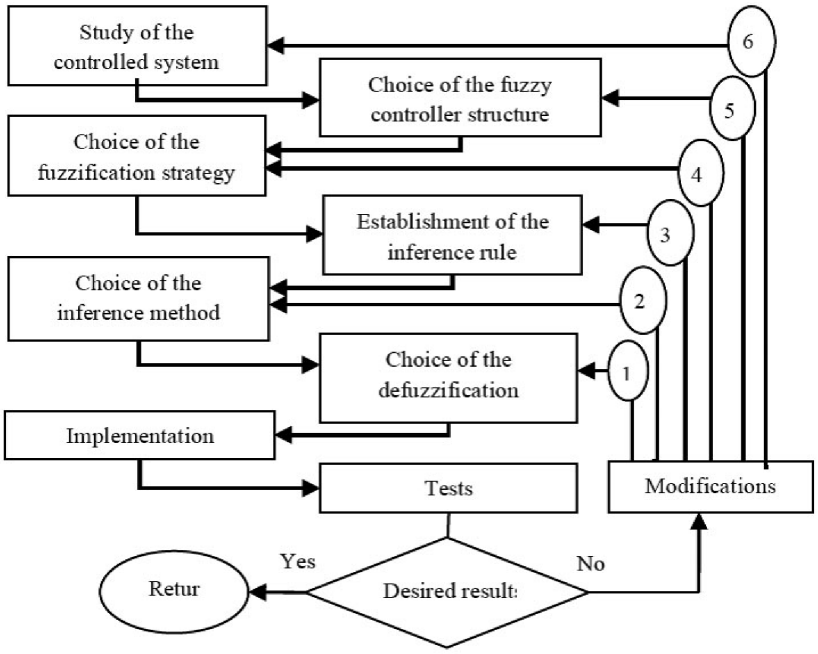

Fig. 9. Flowchart of the FL making process

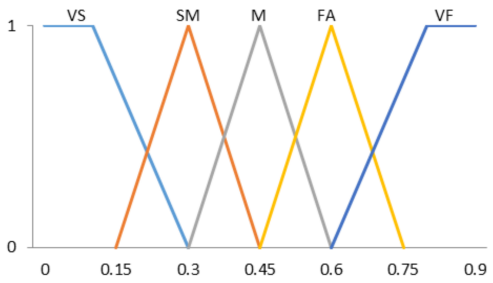

Fig. 10. Membership functions of the input D_{in}

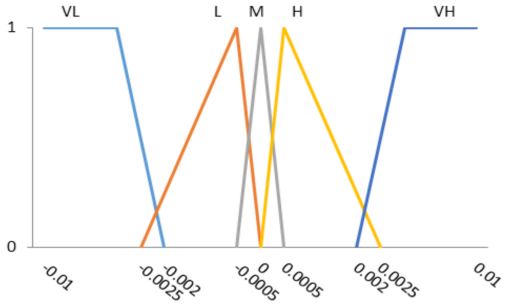

Fig. 11. Membership functions of the Inputs ΔP, ΔV_B and V_B

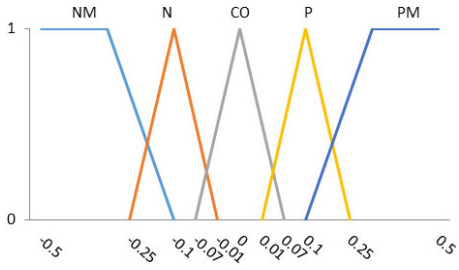

Fig. 12. Membership functions of the output D_{out}

This COG expression is frequently adopted because it makes possible to define analytically the output of the FL system, to simplify its implementation and to reduce the calculation time. Moreover, this definition makes it possible to avoid the discontinuities that could appear in the other methods of defuzzification, in particular the method of Middle-of-Maxima [45].

5. Simulation results

In this section, simulation results are presented and discussed without and with BCR using three different control techniques (P&O-PID, FLC-PID and the proposed Combined FLC (C-FLC)). The used P&O and PID techniques are described in Appendix C and D, respectively. The Simulink block diagram of the EPS and the control strategy is shown in Fig. 13. In this simulation, only the control block is changed. While, the solar cell model and the EPS component are identical in order to maintain the same electrical characteristics allowing a reliable comparison.

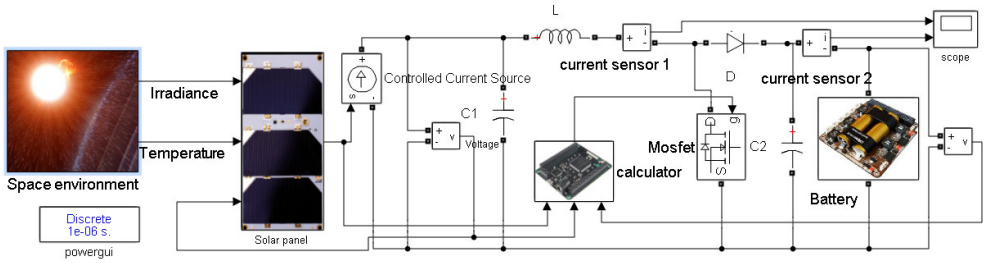

Fig. 13. MATLAB/Simulink implementation of the EPS and control strategy

In this simulation, the most important environmental parameters (irradiance and temperature), which influence the value of the power generated by the PV system, are variable as shown in the Fig. 14.

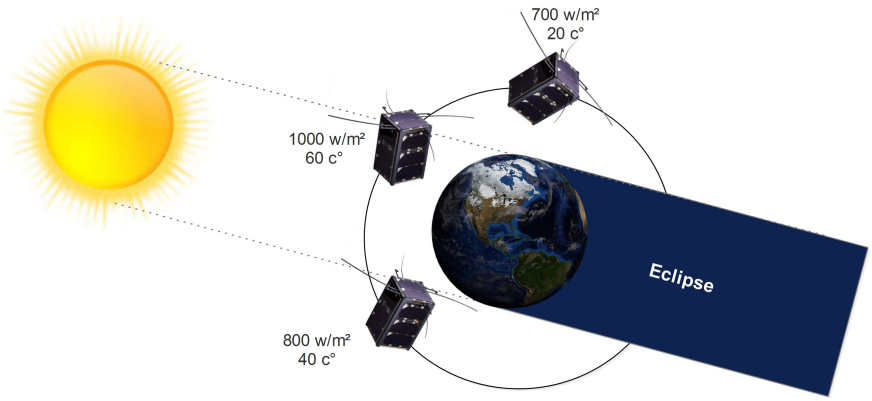

Fig. 14. 1.5U CubeSat in orbit with variation of environmental parameters

Based on the variable attitude (change of angle of attack) of the CubeSat, as shown in Fig. 14, the irradiance and the temperature of solar panels change in orbit. Therefore, in this paper, a hypothesis has been assumed that when the incident solar irradiance is almost normal to the surface (optimal angle of attack) during the sunlight period, the irradiation and the temperature achieve respectively 1000 W/m^2 and 60°C. Otherwise, when different reduced angles of attack are obtained during the period of sunlight, the irradiance and the temperature reach 800 W/m^2 and 40°C and for the lowest irradiance and temperature are 700 W/m^2 and 20°C, respectively.

5.1. Irradiance and temperature variations using the classical techniques without BCR

In order to explain that the implementation of BCR is needed for the EPS, Fig. 15 shows the voltage outputs obtained by different controllers (FLC and P&O).

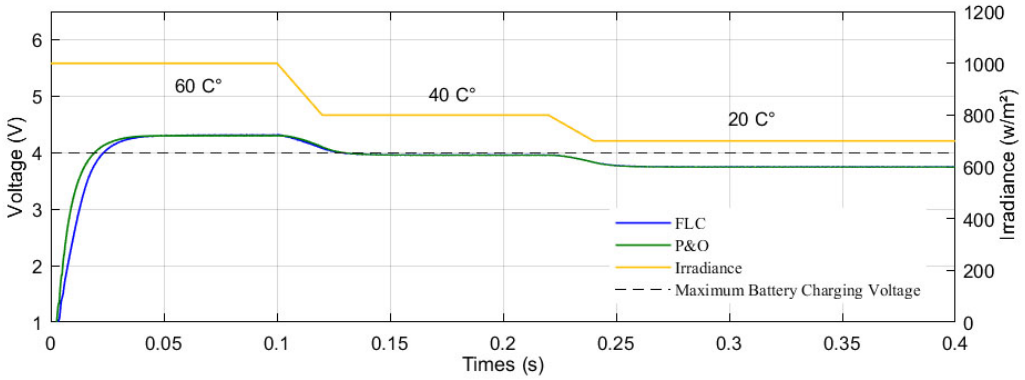

Fig. 15. Output voltages obtained by different MPPT algorithms at different levels of irradiance and temperature without BCR

From Fig. 15, it can be noticed that the output voltage has clearly exceeded the maximum battery charge voltage only when the irradiance and temperature are 1000 W/m^2 and 60°C, respectively. While, when the irradiance and temperature are 800 W/m^2 and 40°C, respectively, the output voltage is just below the rated value and in 700 W/m^2 and 20°C it is very much below the rated value. Therefore, it can be deduced that the BCR must act only when the output voltage has clearly exceeded the maximum battery charge voltage to avoid causes that can damage the battery.

5.2. Irradiance and temperature variations using P&O and FLC with BCR, and the proposed technique C-FLC

The purpose of this test is to analyse the behaviour of the system after implementing the proposed combined FLC that have an internal fuzzy BCR compared to the BCR based on PID control loop with P&O and FLC. The environmental conditions (irradiance and temperature) for validating the proposed C-FLC are chosen, 1000 W/m^2 and 60°C, 800 W/m^2 and 40°C and 700 W/m^2 and 20°C, respectively, in such a way as to have at first a large overshoot on the system response, then just below and at the end greatly below. Fig. 16, Fig. 18 and Fig. 20 show different

magnitudes of the boost outputs, which are power, current and voltage, and, their zooms are shown in Fig. 17, Fig. 19 and Fig. 21.

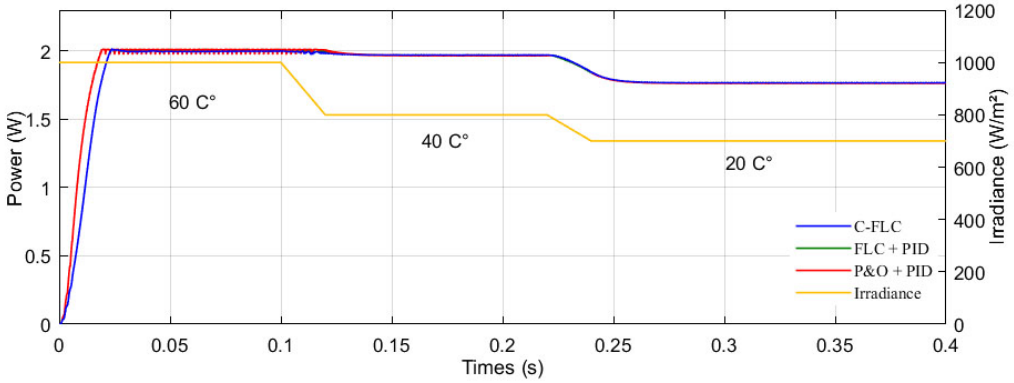

Fig. 16. Output powers obtained by different MPPT algorithms at different levels of irradiance and temperature with BCR

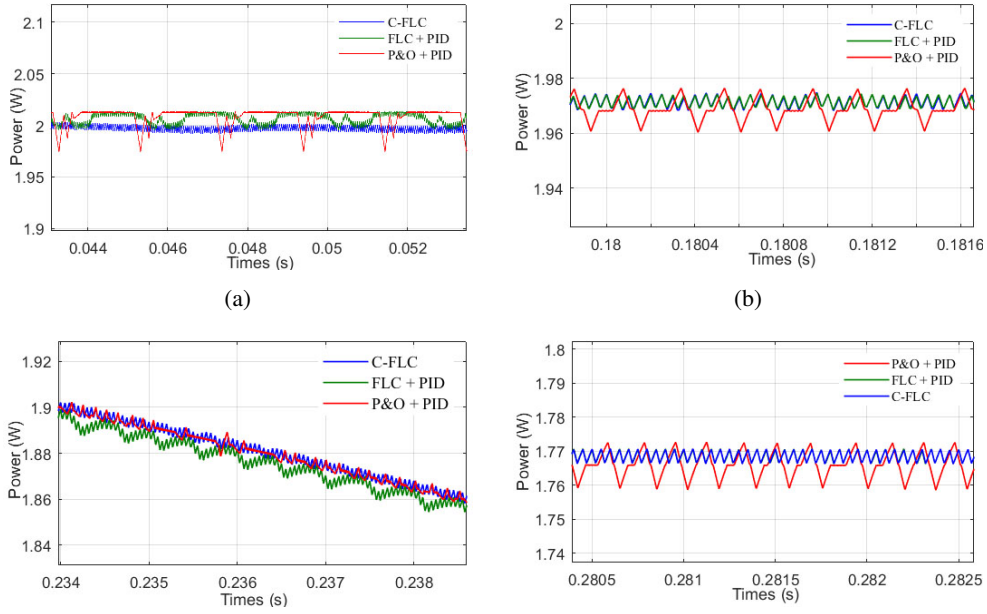

Fig. 17. Zoom of output powers obtained by different algorithms at: constant conditions of 1000 W/m^2 and 60°C (a); constant conditions of 800 W/m^2 and 40°C (b); during change of the conditions from 800 W/m^2 and 40°C to 700 W/m^2 and 20°C (c); constant conditions of 700 W/m^2 and 20°C (d)

According to the simulation results shown in Fig. 16, the powers are clearly reduced with irradiance and temperature at 1 000 W/m^2 and 60°C due to the operation of the BCR. While, in

Fig. 17(a), which is the zoom of output powers obtained at constant conditions of 1000 W/m^2 and 60°C, C-FLC is showing better control performances such as less power oscillations compared to the powers obtained by FLC+PID and P&O+PID. However, as shown in Fig. 17(b), the power obtained by P&O+PID contains higher ripples compared to the powers obtained by C-FLC and FLC+PID that have the same control behaviour with irradiance and temperature at 800 W/m^2 and 40°C and 700 W/m^2 and 20°C, respectively. In Fig. 17(c), it can be noticed that when the conditions pass from 800 W/m^2 and 40°C to 700 W/m^2 and 20°C, compared to the powers obtained by FLC+PID and P&O+PID, C-FLC provides better control performance such as less power ripples. In Fig. 17(d), the same observation seen in Fig. 17(b) is obtained, where the curves C-FLC and FLC+PID are superimposed. Therefore, the similarity of control behaviour between the two controllers (C-FLC and FLC+PID) is noticed just when BCR is not functioning to limit the output voltage of the boost converter to not exceed the maximum battery charge voltage.

The results of the output voltages are illustrated in Fig. 18 and Fig. 19.

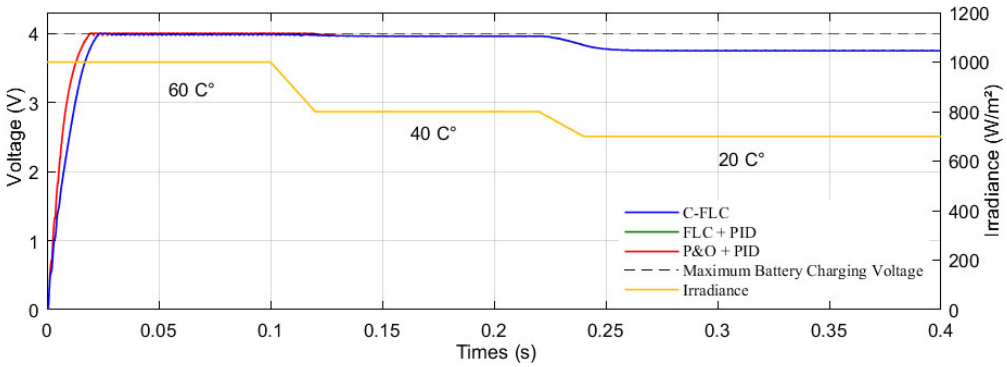

Fig. 18. Output voltages obtained by different MPPT algorithms at different levels of irradiance and temperature with BCR

Unlike the results shown in Fig. 15, due to the BCR function which limits the output voltage of the boost converter, during irradiance and the temperature at 1 000 W/m^2 and 60°C as shown in Fig. 18, the output voltage of the compared algorithms does not exceed the nominal value of the battery voltage. However, from Fig. 19(a), it follows that oscillations around these output signals obtained by P&O+PID and FLC+PID are more important than those obtained by the proposed C-FLC. While, Fig. 19(b), shows that C-FLC and FLC+PID have the same performances when the battery voltage is below the maximum battery voltage and the BCR is not functioning. During the change of the conditions from 800 W/m^2 and 40°C to 700 W/m^2 and 20°C in Fig. 19(c), it is noticeable that the output voltage obtained by P&O+PID contains higher ripples compared to the output voltage obtained by C-FLC and FLC+PID. In Fig. 19(d), it is observed that the BCR is not functioning and the curves of the output voltages obtained by C-FLC and FLC+PID are superimposed. Consequently, it could be deduced that the proposed C-FLC controller is more stable than the other algorithms and thus allows more power with good quality to be stored in batteries that indeed can prolong its lifetime.

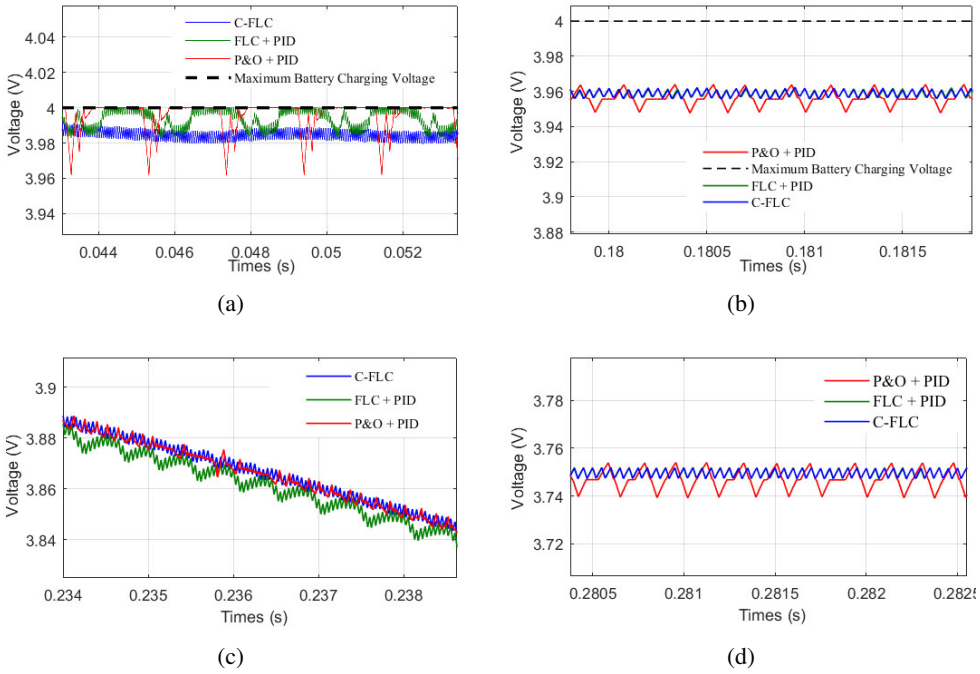

Fig. 19. Zoom of output voltages obtained by different algorithms at: constant conditions of 1000 W/m^2 and 60°C (a); constant conditions of 800 W/m^2 and 40°C (b); during change of the conditions from 800 W/m^2 and 40 °C to 700 W/m^2 and 20°C (c); constant conditions of 700 W/m^2 and 20°C (d)

Current outputs are one of the important electrical characteristics to be analysed for the evaluation of the proposed control technique advantages. Therefore, the results of current outputs are shown in Fig. 20 and Fig. 21.

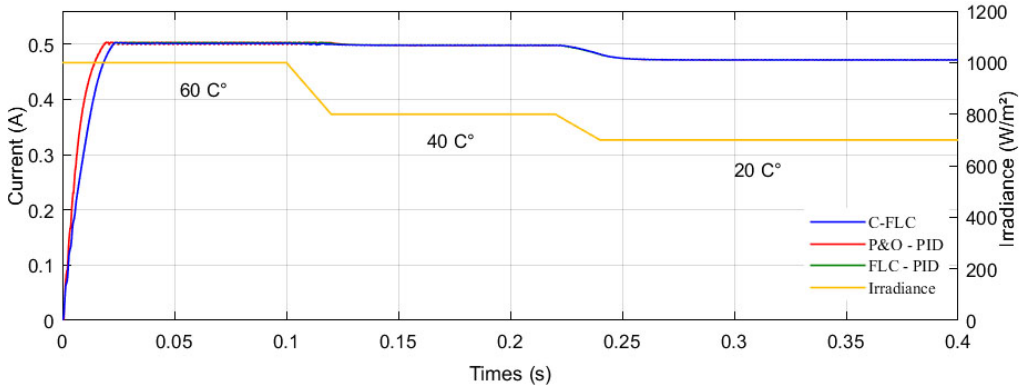

Fig. 20. Output currents obtained by different MPPT algorithms at different levels of irradiance and temperature with BCR

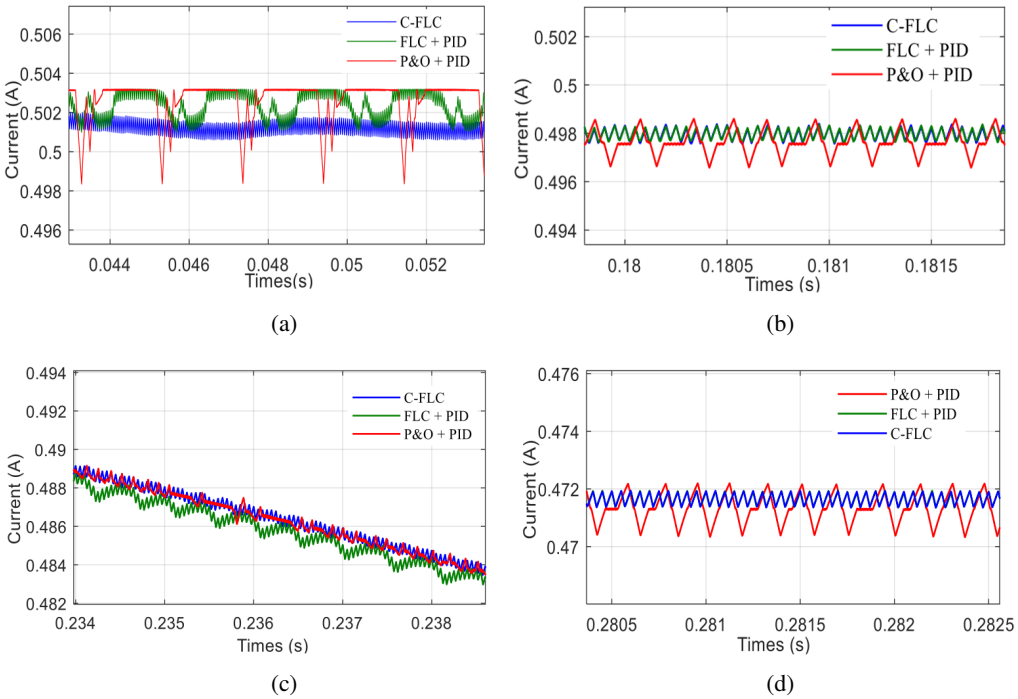

Fig. 21. Zoom of output currents obtained by different algorithms at: constant conditions of 1000 W/m^2 and 60°C (a); constant conditions of 800 W/m^2 and 40°C (b); during change of the conditions from 800 W/m^2 and 40°C to 700 W/m^2 and 20°C (c); constant conditions of 700 W/m^2 and 20°C (d)

From the simulation results shown in Fig. 20 and Fig. 21, it is noticed that the current responses have the same behaviour as power responses, such as less and small oscillations for C-FLC compared to other techniques. This improvement can reduce the effects of internal heating and extend the lifetime of components in electrical circuits.

6. Conclusion

In this paper, the typical Electrical Power System architecture for a CubeSat was modified for the implementation of the proposed combined Fuzzy Logic Control (C-FLC) strategy to simultaneously execute the Maximum Power Point Tracking and Battery Charge Regulator techniques. By simulation (MATLAB / Simulink), this suggested control technique based on C-FLC was tested and compared to other conventional control strategies such as Perturb and Observe (P&O) and FLC with a Proportional Integral Derivative (PID) controller. From the obtained simulation results, in contrast with the conventional control techniques, the proposed control strategy is capable to extract the MPPs, preventing power oscillations and avoid the damage of the battery. In addition, the battery lifespan can be prolonged by reducing the battery current ripples up to three times and also significantly decreases the oscillations of output voltage up to four times as compared to the

system with conventional techniques. Hence, by adopting the C-FLC strategy with the reduced EPS circuit, the reliability and the efficiency of the EPS can be improved. As future work, the proposed combined FLC will be implemented in an FPGA platform; highlighting that the proposed combined FLC can offer the advantage of being precisely controlling the real EPS for CubeSats.

Acknowledgements

I would like to thank the Kyutech laboratory of the Kyushu Institute of Technology for allowing me to use their student MATLAB version with license authorization: 77016046384981527843.

Appendix

Appendix A

In this paper, simulations are investigated with a triple junction solar cell. The parameters of this solar cell are presented in Table 1.

Table 1. Parameters of PV cell [46]

Electrical characteristics	**Values at: Spectrum AM0 WRC = 1367 W/m^2, T = 28°C**
V_{oc}	2.667 V
I_{SC}	0.506 A
R_s	0.546 Ω
K_i	0.32 mA/°C
I_{mpp}	0.487 A
V_{mpp}	2.371 V

Appendix B

Based on [47, 48], the calculated parameters of the boost converter are presented in Table 2.

Table 2. Boost converter parameters

Parameters	**Values**
Inductance *L*	0.00099 H
Capacitor *C1*	0.7 e–4 F
Capacitor *C2*	2 e–3 F
Resistor *R*	7.95 Ohms

Appendix C

The secondary control state consists in regulating the battery voltage at 4 V (or any voltage desired) with a PID controller as shown in Fig. 22. This control loop takes care of the Constant

Fig. 22. Closed loop of battery voltage regulation based on PID controller

Voltage (CV) charging phase of the battery. A switch is included in the system to alternate between the two control states. Then, the small ripple approximation is used to model the boost and design the controller. Based on this assumption, the following transfer function of the boost converter is given as described in [49]:

$$G_v(s) = \frac{v_{dc2}(s)}{\mathrm{d}(s)} = \frac{-I_L \rightleftarrows L \rightleftarrows s + V_{dc2}D'}{C_2Ls^2 + \dfrac{L}{R}s + D'^2}. \tag{10}$$

The calculation of the PID controller parameters is done by the pole placement method.

Appendix D

The P&O method is the MPPT technique most widely used in photovoltaic systems because of its simplicity and easy implementation. The operating principle of this method is to generate a periodic disturbance of the operating voltage and observe its effect on the output power. The flowchart of the P&O algorithm is illustrated in Fig. 23.

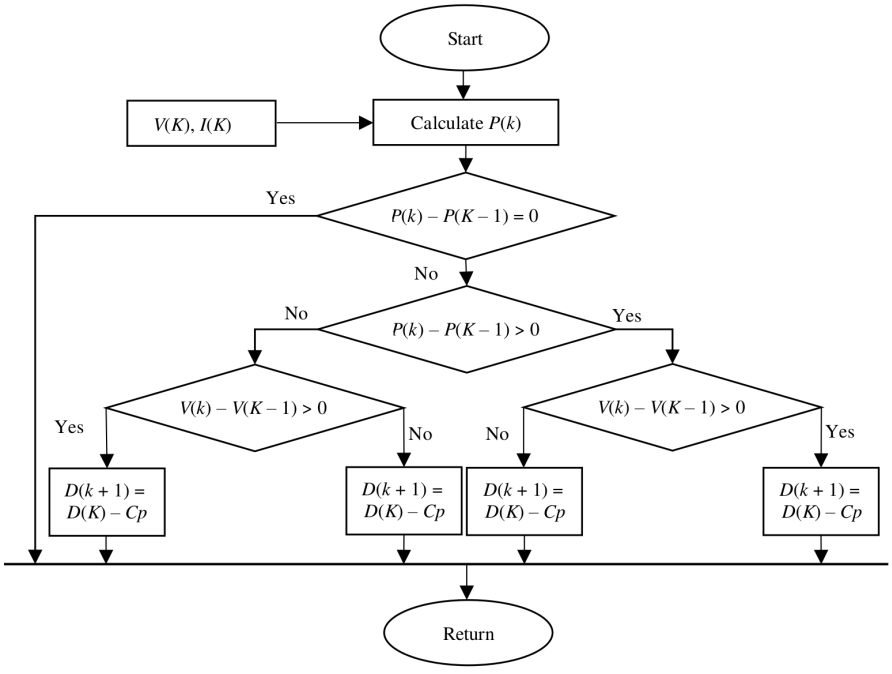

Fig. 23. P&O MPPT algorithm flowchart

Appendix E

A total of 50 rules used for the proposed combined FLC are shown in Table 3, where inputs 1, 2, 3, and 4 are ΔP, D_{in}, V_B and $\Delta V_B(K)$ and the output is D_{out}.

Table 3. Fuzzy rules for the proposed combined FLC

ΔP	D_{in}	V_B			$\Delta V_B(K)$		D_{out}	ΔP	D_{in}	V_B	$\Delta V_B(K)$	D_{out}
1	1	1	2	3	1	2	3	1	1	4	1	1
1	2	1	2	3	1	2	3	1	2	4	2	1
1	3	1	2	3	1	2	3	1	3	4	3	2
1	4	1	2	3	1	2	4	1	4	4	4	3
1	5	1	2	3	1	2	5	1	5	4	5	3
2	1	1	2	3	1	2	2	2	1	5	1	1
2	2	1	2	3	1	2	2	2	2	5	2	1
2	3	1	2	3	1	2	3	2	3	5	3	2
2	4	1	2	3	1	2	4	2	4	5	4	2
2	5	1	2	3	1	2	5	2	5	5	5	3
3	1	1	2	3	1	2	1	3	1	5	1	1
3	2	1	2	3	1	2	3	3	2	5	2	1
3	3	1	2	3	1	2	3	3	3	5	3	2
3	4	1	2	3	1	2	4	3	4	5	4	2
3	5	1	2	3	1	2	5	3	5	5	5	3
4	1	1	2	3	1	2	1	4	1	5	1	1
4	2	1	2	3	1	2	2	4	2	5	2	1
4	3	1	2	3	1	2	3	4	3	5	3	2
4	4	1	2	3	1	2	3	4	4	5	4	2
4	5	1	2	3	1	2	4	4	5	5	5	3
5	1	1	2	3	1	2	1	5	1	5	1	1
5	2	1	2	3	1	2	2	5	2	5	2	1
5	3	1	2	3	1	2	3	5	3	5	3	2
5	4	1	2	3	1	2	3	5	4	5	4	2
5	5	1	2	3	1	2	3	5	5	5	5	3

References

[1] Poghosyan A., Golkar A., *CubeSat evolution: Analyzing CubeSat capabilities for conducting science missions*, Progress in Aerospace Sciences, vol. 88, pp. 59–83 (2017).

[2] Fritz B.A., Stephan A.W., Walker P.W., Brown C.M., Nicholas A.C., Dymond K.F., Budzien S.A., Marquis P.J., Finne T.T., Wolfram K.D., *Ultraviolet beam splitter characterization for use in a CubeSat optical system*, Journal of Applied Remote Sensing, vol. 13, no. 3, p. 032503 (2019).

[3] Garcia R.F., Sibbing Z.R., Van Camp A., *Can We Estimate Air Density of the Thermosphere with CubeSats*?, Journal of Spacecraft and Rockets, pp. 1–8 (2019).

[4] Song S., Kim H., Chang Y.-K., *Design and Implementation of 3U CubeSat Platform Architecture*, International Journal of Aerospace Engineering, vol. 1, pp. 1–17 (2018), DOI: 10.1155/2018/2079219.

[5] https://www.endurosat.com/cubesat-store/all-cubesat-modules/1-5u-cubesat-platform/, accessed 2019.

[6] Xu D., Zhang D., *Power Electronics Systems in Satellites*, Control of Power Electronic Converters and Systems, edited by: Elsevier (2018).

[7] Kerrouche K., Wang L., Aoudeche A., *Low-Cost EPS for nanosatellites constellation of belt and road countries*, Fourth IAA Conference on Dynamics and Control of Space Systems, DyCoSS (2018).

[8] Peng L., Jun Z., Xiaozhou Y., Luping C., *Design and validation of modular MPPT electric power system for multi-U CubeSat*, 2017 3rd IEEE International Conference on Control Science and Systems Engineering (ICCSSE), pp. 374–377 (2017).

[9] Ahmed J., Salam Z., *A modified P&O maximum power point tracking method with reduced steady-state oscillation and improved tracking efficiency*, IEEE Transactions on Sustainable Energy, vol. 7, no. 4, pp. 1506–1515 (2016).

[10] Ballaji A., Divakar B., Hediyal N., Mandi R.P., Swamy K.N., *Energy Efficient Perturb and Observe Maximum Power Point Algorithm with Moving Average Filter for Photovoltaic Systems*, International Journal of Renewable Energy Research, vol. 9, no. 1 (2019).

[11] Belkaid A., Colak I., Kayisli K., *Implementation of a modified P&O-MPPT algorithm adapted for varying solar radiation conditions*, Electrical Engineering, vol. 99, no. 3, pp. 839–846 (2017).

[12] Gopal Y., Kumar K., Birla D., Lalwani M., *Banes and boons of perturb and observe, incremental conductance and modified regula falsi methods for sustainable PV energy generation*, Journal of Power Technologies, vol. 97, no. 1, pp. 35–43 (2017).

[13] Isaloo B.A., Amiri P., *Improved variable step size incremental conductance MPPT method with high convergence speed for PV systems*, Journal of Engineering Science and Technology, vol. 11, no. 4, pp. 516–528 (2016).

[14] Loukriz A., Haddadi M., Messalti S., *Simulation and experimental design of a new advanced variable step size Incremental Conductance MPPT algorithm for PV systems*, ISA transactions, vol. 62, pp. 30–38 (2016).

[15] Zakzouk N.E., Elsaharty M.A., Abdelsalam A.K., Helal A.A., Williams B.W., *Improved performance low-cost incremental conductance PV MPPT technique*, IET Renewable Power Generation, vol. 10, no. 4, pp. 561–574 (2016).

[16] Bartczak M., *Partial Shading Detection in Solar System Using Single Short Pulse of Load*, Metrology and Measurement Systems, vol. 24, no. 1, pp. 193–199 (2017).

[17] Bendib B., Krim F., Belmili H., Almi M., Boulouma S., *Advanced Fuzzy MPPT Controller for a stand-alone PV system*, Energy Procedia, vol. 50, pp. 383–392 (2014).

[18] Samal S., Barik P.K., Sahu S.K., *Extraction of maximum power from a solar PV system using fuzzy controller based MPPT technique*, 2018 Technologies for Smart-City Energy Security and Power (ICSESP), pp. 1–6 (2018).

[19] Jasim A., Shepetov Y., *Maximum Power Point Tracking for Satellite Solar Power Load Matching under Different Light Panels*, Current Journal of Applied Science and Technology, pp. 1–14 (2017).

[20] Talha A., Boumaaraf H., Bouhali O., *Evaluation of maximum power point tracking methods for photovoltaic systems*, Archives of Control Sciences, vol. 21, no. 2, pp. 151–165 (2011).

[21] Cardozo D.O., Pardo M., Algarín C.R., *Fuzzy Logic Controller for Maximum Power Point Tracking Based on Voltage Error Measurement in Isolated Photovoltaic Systems*, 2018 IEEE ANDESCON, pp. 1–6 (2018).

[22] Wang Y., Yang Y., Fang G., Zhang B., Wen H., Tang H., Fu L., Chen X., *An Advanced Maximum Power Point Tracking Method for Photovoltaic Systems by Using Variable Universe Fuzzy Logic Control Considering Temperature Variability*, Electronics, vol. 7, no. 12, p. 355 (2018).

[23] Yilmaz U., Kircay A., Borekci S., *PV system fuzzy logic MPPT method and PI control as a charge controller*, Renewable and Sustainable Energy Reviews, vol. 81, pp. 994–1001 (2018).

[24] Mlakić D., Nikolovski S., *ANFIS as a method for determinating MPPT in the photovoltaic system simulated in MATLAB/Simulink*, 2016 39th International Convention on Information and Communication Technology, Electronics and Microelectronics (MIPRO), pp. 1082–1086 (2016).

[25] Della Krachai S., Stambouli A.B., Della Krachai M., Bekhti M., *Experimental investigation of artificial intelligence applied in MPPT techniques*, International Journal of Power Electronics and Drive Systems, vol. 10, no. 4, p. 2138 (2019).

[26] Hassan S., Li H., Kamal T., Arifoğlu U., Mumtaz S., Khan L., *Neuro-Fuzzy wavelet based adaptive MPPT algorithm for photovoltaic systems*, Energies, vol. 10, no. 3, p. 394 (2017).

[27] Bahri O., Talbi E.-G., Amor N.B., *A generic fuzzy approach for multi-objective optimization under uncertainty*, Swarm and Evolutionary Computation, vol. 40, pp. 166–183 (2018).

[28] Seddjar A., Berrached N., *A Fuzzy Approach for a Hybrid Multi-Mobile Robot Control Architecture to Maintain a Specific Formation During Navigation*, International Review of Automatic Control (IREACO), vol. 8, no. 1, pp. 63–71 (2015).

[29] Shiau J.-K., Wei Y.-C., Lee M.-Y., *Fuzzy controller for a voltage-regulated solar-powered MPPT system for hybrid power system applications*, Energies, vol. 8, no. 5, pp. 3292–3312 (2015).

[30] Neji B., Hamrouni C., Alimi A.M., Nakajima H., Alim A.R., *Hierarchical Fuzzy-Logic-Based Electrical Power Subsystem for Pico Satellite ERPSat-1*, IEEE Systems Journal, vol. 9, no. 2, pp. 474-486 (2013).

[31] Naick K., Chatterjee K., Chatterjee T., *Fuzzy logic controller based maximum power point tracking technique for different configurations of partially shaded photovoltaic system*, Archives of Electrical Engineering (2018).

[32] Bhat Nempu P., Sabhahit Jayalakshmi N., *A new power management strategy for PV-FC-based autonomous DC microgrid*, Archives of Electrical Engineering, vol. 67, no. 4 (2018).

[33] Drir N., Barazane L., Loudini M., *Optimizing the operation of a photovoltaic generator by a genetically tuned fuzzy controller*, Archives of Control Sciences, vol. 23, no. 2, pp. 145–167 (2013).

[34] Krause F.C., Loveland J.A., Smart M.C., Brandon E.J., Bugga R.V., *Implementation of commercial Li-ion cells on the MarCO deep space CubeSats*, Journal of Power Sources, vol. 449, p. 227544 (2020).

[35] Sanchez-Sanjuan S., Gonzalez-Llorente J., Hurtado-Velasco R., *Comparison of the incident solar energy and battery storage in a 3U CubeSat satellite for different orientation scenarios*, Journal of Aerospace Technology and Management, vol. 8, no. 1, pp. 91–102 (2016).

[36] Gonzalez-Llorente J., Lidtke A.A., Hurtado R., Okuyama K.-I., *Single-Bus and Dual-Bus Architectures of Electrical Power Systems for Small Spacecraft*, Journal of Aerospace Technology and Management, vol. 11 (2019).

[37] Bogaraj T., Kanakaraj J., Chelladurai J., *Modeling and simulation of stand-alone hybrid power system with fuzzy MPPT for remote load application*, Archives of Electrical Engineering, vol. 64, no. 3, pp. 487–504 (2015).

[38] Shah M., Juneja A., Bhattacharya S., Dean A.G., *High frequency GaN device-enabled CubeSat EPS with real-time scheduling*, 2012 IEEE Energy Conversion Congress and Exposition (ECCE), pp. 2934–2941 (2012).

[39] Mojallizadeh M.R., Karimi B., *Nonlinear control of a satellite electrical power system based on the sliding mode control*, ISRN Aerospace Engineering, vol. 2013 (2013).

[40] Villalva M.G., Gazoli J.R., Ruppert Filho E., *Comprehensive approach to modeling and simulation of photovoltaic arrays*, IEEE Transactions on Power Electronics, vol. 24, no. 5, pp. 1198–1208 (2009).

[41] Rekioua D., Matagne E., *Optimization of photovoltaic power systems: modelization, simulation and control*, Springer Science and Business Media (2012), DOI: 10.1007/978-1-4471-2403-0.

[42] Initiative N.C.L., *CubeSat 101: Basic Concepts and Processes for First-Time CubeSat Developers*, San Luis Obispo, USA (2017).

[43] Dadios E., *Fuzzy Logic: Controls, Concepts, Theories and Applications*, BoD–Books on Demand (2012).

[44] Rahim R., *Comparative Analysis of Membership Function on Mamdani Fuzzy Inference System for Decision Making*, Journal of Physics Conference Series, vol. 930 (2017).

[45] Iancu I., *A Mamdani type fuzzy logic controller*, Fuzzy Logic-Controls, Concepts, Theories and Applications, edited by: IntechOpen (2012), DOI: 10.5772/36321.

[46] *GmbH A.S.S.P., 28% Triple Junction GaAs Solar Cell Type: TJ Solar Cell 3G28C*, edited (2016).

[47] Mohan N., *Power electronics: a first course*, Wiley (2011).

[48] Motahhir S., El Ghzizal A., Sebti S., Derouich A., *MIL and SIL and PIL tests for MPPT algorithm*, Cogent Engineering, vol. 4, no. 1, p. 1378475 (2017).

[49] Erickson R.W., Maksimovic D., *Fundamentals of power electronics*, Springer Science and Business Media (2007).